Gauge-invariant theory of quasiparticle and condensate dynamics in response to terahertz optical pulses in superconducting semiconductor quantum wells. II. ($s + p$)-wave superconductivity in the strong spin-orbit coupling limit

T. Yu* and M. W. Wu†

Hefei National Laboratory for Physical Sciences at Microscale, Department of Physics, and CAS Key Laboratory of Strongly-Coupled Quantum Matter Physics, University of Science and Technology of China, Hefei, Anhui, 230026, China

(Received 21 August 2017; published 31 October 2017)

We investigate the quasiparticle and condensate dynamics in response to the terahertz (THz) optical pulses in the strong spin-orbit-coupled ($s + p$)-wave superconducting semiconductor quantum wells by using the gauge-invariant optical Bloch equations in the quasiparticle approximation. Both the dynamics of triplet and singlet superconductivity are studied in response to the THz optical pulses. Specifically, for the triplet superconductivity, we predict that in the ($s + p$)-wave superconducting (100) quantum wells, with the vector potential parallel to the quantum wells, the optical field can cause the total spin polarization of Cooper pairs, oscillating with the frequency of the optical field. The direction of the total Cooper-pair spin polarization is shown to be parallel to the vector potential. For the singlet superconductivity, we show that due to the large spin-orbit coupling in InSb (100) quantum wells, there exist two Fermi surfaces including the inner and outer ones. In this specific configuration, the superconducting momentum can be tuned to be larger than the inner Fermi momentum but smaller than the outer one. We find that in this regime, the dynamics of the Higgs mode and charge imbalance shows different features in comparison with the conventional s-wave case.

DOI: 10.1103/PhysRevB.96.155312

I. INTRODUCTION

The gauge-invariant theory of quasiparticle and condensate dynamics in response to terahertz (THz) optical pulses in the weak spin-orbit-coupled s-wave superconducting semiconductor quantum wells has been discussed in the previous paper of this series [1], which is referred to as Part I in the following. In Part I [1], we have shown that the superfluid velocity can be induced by the optical field, which itself can contribute to the pump of quasiparticles (pump effect). Moreover, the rate of change of the induced superfluid velocity can act as the drive field to drive the quasiparticles (drive effect). Specifically, we find that the oscillations of the Higgs mode with twice the frequency of the optical field is dominantly contributed by the drive effect but not the pump effect as long as the driven superconducting momentum is less than the Fermi momentum. Furthermore, from the charge-neutrality condition, we predict that during the optical process, the quasiparticle charge imbalance can be induced by the pump and drive effects separately, leading to the fluctuation of the chemical potential for the condensate.

It is noted that in the above conventional s-wave superconductivity, the Cooper pairs do not carry any net spin. As the optical method is often used to create and manipulate the electron spins in semiconductors [2–5] or topological insulator [6] by inducing an effective spin-orbit coupling (SOC), it is intriguing to consider the possibility of the creation and manipulation for the Cooper-pair spin polarization in superconductor. This is possible in the triplet superconductivity as the triplet Cooper pairs can carry net spin polarization [7–12]. For the triplet superconductivity, there exist three vectors in the literature to describe its equilibrium and nonequilibrium properties from the microscopic viewpoint to the macroscopic one [7,13–16]. In the microscopic level, the triplet superconductivity is described by the triplet Cooper pairing, which can be defined as $[\mathbf{f}(\mathbf{k},\omega)\cdot\boldsymbol{\sigma}]i\sigma_y$ by using the $\mathbf{f}$ vector [7,14–16]. Here, $\boldsymbol{\sigma} = (\sigma_x,\sigma_y,\sigma_z)$ denotes the Pauli matrices. It can be seen that the $\mathbf{f}$ vector is frequency and momentum dependent [7,14–16]. Then, with the information of the frequency integrated, the triplet superconductivity is described by the triplet anomalous correlation, which can be defined as $[\mathbf{l}(\mathbf{k})\cdot\boldsymbol{\sigma}]i\sigma_y$ by using the $\mathbf{l}$ vector [13]. Finally, in the macroscopic level, with the momentum further integrated in the gap equation, the triplet superconductivity is described by the triplet order parameter, which can be defined as $[\mathbf{d}(\mathbf{k})\cdot\boldsymbol{\sigma}]i\sigma_y$ by using the $\mathbf{d}$ vector [13].

One sees that the inclusion of the optical field can break the time-reversal symmetry. Previous works have shown that the breaking of the time-reversal symmetry by the Zeeman field [17] or the supercurrent [16] can induce the Cooper-pair spin polarization. In the former situation, for the conventional s-wave superconductor in proximity to a ferromagnet, the triplet Cooper pairing can be induced in the superconductor-ferromagnet interface [9,18–23]. Then, Jacobsen *et al.* showed that in the superconductor-ferromagnet-superconductor Josephson junction, when there exists the SOC in the superconductor-ferromagnet interface, the net spin polarization of triplet Cooper pairs can be created, and a superconducting spin flow with spin-flip immunity can be realized [17]. In the latter situation, Tkachov pointed out that in noncentrosymmetric superconductors, a *nonunitary* triplet pairing [7,13,14] can be induced by the supercurrent, which contributes to the spin polarization of triplet Cooper pairs and can be detected by the magnetoelectric Andreev effect [16].

It is noted that Tkachov's calculation is performed in the static situation, in which the supercurrent is induced

*taoyuphy@mail.ustc.edu.cn
†mwwu@ustc.edu.cn

from the proximity effect [16]. Nevertheless, in the system with strong SOC, with the superfluid velocity dynamically generated by the optical field, we expect that the Cooper-pair spin polarization can also be induced, which has not yet been reported in the literature. Particularly, the optical method can avoid the complexity when introducing the supercurrent by the proximity effect. Furthermore, the study of the dynamics of the Cooper-pair spin polarization can provide more understanding from the microscopic point of view.

In this work, we investigate the optical response to the THz pulses in the strong spin-orbit-coupled $(s+p)$-wave superconducting semiconductor QWs. The gauge-invariant optical Bloch equations in the quasiparticle approximation are set up via the gauge-invariant nonequilibrium Green function approach [24–30], in which the gauge-invariant Green function with the Wilson line [25–27,31] is constructed by using the gauge structure revealed by Nambu [32]. Both the dynamics of triplet and singlet superconductivity are studied in response to the THz optical pulses. Specifically, for the triplet superconductivity, we first show the Cooper-pair spin polarization can be described by the $\mathbf{l}$ vector, which can be seen as follows.

Here, the $\mathbf{l}$ vector is further written as

$$[\mathbf{l}(\mathbf{k})\cdot\boldsymbol{\sigma}]i\sigma_y=\begin{pmatrix}F_{\uparrow\uparrow}(\mathbf{k}) & F_{\uparrow\downarrow}(\mathbf{k})\\ F^*_{\uparrow\downarrow}(\mathbf{k}) & F_{\downarrow\downarrow}(\mathbf{k})\end{pmatrix}, \tag{1}$$

with $F(\mathbf{k})$ representing the anomalous correlations of *triplet* Cooper pairs [13]. Actually, the anomalous correlations $F(\mathbf{k})$, calculated by the optical Bloch equations in this work, are just the Fourier components of the wave function of triplet Cooper pairs in the spatial space [13]. By further considering the spin space, the wave function of the triplet Cooper pairs is expressed as [13]

$$\begin{aligned}F_t(\mathbf{r})=&F_{\uparrow\uparrow}(\mathbf{r})|\uparrow_1\rangle|\uparrow_2\rangle+F_{\downarrow\downarrow}(\mathbf{r})|\downarrow_1\rangle|\downarrow_2\rangle\\&+F_{\uparrow\downarrow}(\mathbf{r})(1/\sqrt{2})\big(|\uparrow_1\rangle|\downarrow_2\rangle+|\downarrow_1\rangle|\uparrow_2\rangle\big).\end{aligned} \tag{2}$$

Here, $F_{\uparrow\uparrow}(\mathbf{r})$, $F_{\downarrow\downarrow}(\mathbf{r})$, and $F_{\uparrow\downarrow}(\mathbf{r})$ denote the wave functions of the triplet Cooper pairs with total spin $S_z=1,-1$, and 0 [13], respectively, with $\mathbf{r}$ being the relative coordinate for the two electrons (labeled by "1" and "2") in the Cooper pairs. Thus, with the $\hat{\mathbf{z}}$ direction of the spin operator chosen to be perpendicular to the quantum wells (QWs), in the equilibrium state of superconducting InSb (100) QWs, $F_{\uparrow\downarrow}(\mathbf{r})=0$ and $|F_{\uparrow\uparrow}(\mathbf{r})|=|F_{\downarrow\downarrow}(\mathbf{r})|$ [33]. From the Cooper-pair wave function, the total spin polarization of Cooper pairs is determined by

$$\mathbf{P}_{\mathrm{C}}=\int d\mathbf{r}\,F_t^*(\mathbf{r})\hat{\mathbf{S}}F_t(\mathbf{r})\propto\sum_{\mathbf{k}}i\mathbf{l}(\mathbf{k})\times\mathbf{l}^*(\mathbf{k}), \tag{3}$$

with $\hat{\mathbf{S}}\equiv\hat{\mathbf{s}}_1+\hat{\mathbf{s}}_2$ being the total spin operator by the sum of the spin operators $\hat{\mathbf{s}}_1$ and $\hat{\mathbf{s}}_2$ of two electrons.

We then predict that in the strong spin-orbit-coupled $(s+p)$-wave superconducting InSb (100) QWs, with the vector potential being along the $\hat{\mathbf{x}}$ direction, the optical field can cause the spin polarization of Cooper pairs, which is also along the $\hat{\mathbf{x}}$ direction and oscillates with the frequency of the optical field. Specifically, in our previous work, it has been revealed that in InSb (100) QWs in proximity to an s-wave superconductor, due to the Dresselhaus SOC, there exists p-wave triplet Cooper correlation in $(p_x\pm ip_y)$ type [33]. In the equilibrium state, the $\mathbf{l}$ vector of the triplet Cooper correlation is parallel to the effective magnetic field $\boldsymbol{\Omega}(\mathbf{k})$ due to the SOC in the momentum space. When the optical field with the vector potential along the $\hat{\mathbf{x}}$ direction is applied to the superconducting system, the superconducting velocity is induced, which is shown to contribute to an effective SOC along the $\hat{\mathbf{x}}$ direction. This effective SOC can cause the precession of the $\mathbf{l}$ vectors, with a component perpendicular to $\boldsymbol{\Omega}(\mathbf{k})$ induced. Thus, with the Cooper-pair spin vector defined as $\mathbf{n}(\mathbf{k})=i\mathbf{l}(\mathbf{k})\times\mathbf{l}^*(\mathbf{k})$ [7,14–16], whose momentum integral contributes to the total Cooper-pair spin polarization $\mathbf{P}_{\mathrm{C}}$ [refer to Eq. (3)], the $\hat{\mathbf{x}}$ component of $\mathbf{P}_{\mathrm{C}}$ can be induced. Specifically, the $\hat{\mathbf{x}}$ component of the Cooper-pair spin polarization is $\mathbf{P}^x_{\mathrm{C}}=(1/\sqrt{2})\int d\mathbf{r}\{F^*_{\uparrow\downarrow}(\mathbf{r})[F_{\uparrow\uparrow}(\mathbf{r})+F_{\downarrow\downarrow}(\mathbf{r})]+\mathrm{H.c.}\}$. Accordingly, one finds that the excitation of the $\hat{\mathbf{x}}$ component of the Cooper-pair spin polarization is the reflection of the optical induction of the triplet Cooper-pair wave function $F_{\uparrow\downarrow}(\mathbf{r})$ with $S_z=0$. Actually, the Fourier component of $F_{\uparrow\downarrow}(\mathbf{r})$ is exactly $\mathbf{l}_z(\mathbf{k})$ [7,14–16]. Furthermore, we reveal that the Cooper-pair spin polarization is proportional to the superconducting velocity, which oscillates with the frequency of the optical field.

For the singlet superconductivity, we study the dynamics of the Higgs mode and charge imbalance induced by the optical field. We show that with typical electron density in InSb (100) QWs, due to the strong SOC, the specific band structure results in two Fermi surfaces, including the the inner and outer ones. Thus, the superconducting momentum can be tuned to be larger than the inner Fermi momentum but smaller than the outer one. We find that in this regime, the dynamics of the Higgs mode and charge imbalance shows different features in comparison with the conventional s-wave case (refer to Part I [1]). Specifically, we find that in this regime, the pump effect can indeed have contribution to the excitation of the Higgs mode, which has been shown to play a negligible role in the s-wave case in Part I [1]. Moreover, in this regime, we reveal that there exists interplay between the pump and drive effects in the excitation of the charge imbalance.

This paper is organized as follows. We first generalize the framework in the weak spin-orbit-coupled s-wave superconducting semiconductor QWs in Part I [1] to the strong spin-orbit-coupled $(s+p)$ wave one in (100) QWs in Sec. II. Specifically, we present the Hamiltonian in Sec. II A; then in Sec. II B, the optical Bloch equations derived via the gauge-invariant nonequilibrium Green function approach are presented. The numerical results are presented in Sec. III. We summarize in Sec. IV.

II. HAMILTONIAN AND OPTICAL BLOCH EQUATIONS

In this section, we study the optical response to the THz pulses in the $(s+p)$-wave superconducting QWs, which can be realized in the strong spin-orbit-coupled InSb (100) QWs in proximity to an s-wave superconductor [33,34]. In the symmetric (100) QWs, the SOC is contributed by the Dresselhaus SOC, whose effective magnetic field is expressed as [33]

$$\boldsymbol{\Omega}_{\mathbf{k}}=-\alpha k_x\hat{\mathbf{x}}+\alpha k_y\hat{\mathbf{y}}. \tag{4}$$

One sees that there only exist in-plane components in the effective magnetic field. In our previous work [33], we have shown that in this configuration, due to the Dresselhaus SOC, not only the p-wave triplet Cooper pairing but also the corresponding triplet order parameter can be induced, which are in $(p_x \pm ip_y)$ type. Moreover, we find that in the momentum space, the $\mathbf{l}$ vector for the triplet anomalous correlation and $\mathbf{d}$ vector for the triplet order parameter are parallel to the effective magnetic field $\mathbf{\Omega_k}$ due to the SOC (refer to Fig. 5 in Ref. [33]). A similar configuration can also be realized in $CePt_3Si$ superconducting film, which is a heavy-fermion material [35–37].

Here, based on the understanding on the equilibrium properties of $(s+p)$-wave superconductor [33–37], it is intriguing to explore their nonequilibrium properties, especially those of the triplet Cooper pairs. Below, we first present the Hamiltonian and then extend the gauge-invariant optical Bloch equations in the s-wave case to the $(s+p)$-wave one.

A. Hamiltonian

In the $(s+p)$-wave superconducting (100) QWs, the Hamiltonian is composed by the free BdG Hamiltonian $\tilde{H}_0$ and the interaction Hamiltonian including the electron-electron Coulomb and electron-impurity interactions $\tilde{H}_{\rm ee}$ and $\tilde{H}_{\rm ei}$. Here, the electron-phonon interaction is neglected due to its weak contribution at the low temperature (refer to Part I [1]). Specifically, the free BdG Hamiltonian in the presence of an optical field propagating along the $\hat{\mathbf{z}}$ direction, in which the vector potential is assumed to be along the $\hat{\mathbf{x}}$ direction, is written as [24,37]

$$\tilde{H}_0 = \int \frac{d\mathbf{r}}{2} \tilde{\Psi}^\dagger \begin{pmatrix} \frac{(\mathbf{p}-\frac{e}{c}\mathbf{A})^2}{2m^*} - \mu + e\phi(x) & -\alpha(k_x - \frac{eA_x}{c}) - i\alpha k_y & \frac{\Delta_p}{2}\{e^{i\zeta(x)}, e^{i\theta_{\mathbf{k}}}\} & \Delta_s e^{i\zeta(x)} \\ -\alpha(k_x - \frac{eA_x}{c}) + i\alpha k_y & \frac{(\mathbf{p}-\frac{e}{c}\mathbf{A})^2}{2m^*} - \mu + e\phi(x) & -\Delta_s e^{i\zeta(x)} & -\frac{\Delta_p}{2}\{e^{i\zeta(x)}, e^{-i\theta_{\mathbf{k}}}\} \\ \frac{\Delta_p}{2}\{e^{-i\zeta(x)}, e^{-i\theta_{\mathbf{k}}}\} & -\Delta_s e^{-i\zeta(x)} & -\frac{(\mathbf{p}+\frac{e}{c}\mathbf{A})^2}{2m^*} + \mu - e\phi(x) & -\alpha(k_x + \frac{eA_x}{c}) + i\alpha k_y \\ \Delta_s e^{-i\zeta(x)} & -\frac{\Delta_p}{2}\{e^{-i\zeta(x)}, e^{i\theta_{\mathbf{k}}}\} & -\alpha(k_x + \frac{eA_x}{c}) - i\alpha k_y & -\frac{(\mathbf{p}+\frac{e}{c}\mathbf{A})^2}{2m^*} + \mu - e\phi(x) \end{pmatrix} \tilde{\Psi}. \quad (5)$$

Here, $\tilde{\Psi}(x) = (\psi_\uparrow(x), \psi_\downarrow(x), \psi_\uparrow^\dagger(x), \psi_\downarrow^\dagger(x))$ represents the field operator in the Nambu $\otimes$ spin space; $\alpha = \gamma_D(\pi/a)^2$ for the infinitely deep well with γ_D being the Dresselhaus coefficient and a representing the well width; and Δ_p (Δ_s) is the magnitude of the p-wave triplet (s-wave singlet) order parameter. The electron-electron Coulomb and electron-impurity interactions are written as

$$\tilde{H}_{\rm ee} = \int \frac{d\mathbf{r}\, d\mathbf{r}'}{8} U(\mathbf{r}-\mathbf{r}')[\tilde{\Psi}^\dagger(\mathbf{r})\mathcal{T}_3\tilde{\Psi}(\mathbf{r})][\tilde{\Psi}^\dagger(\mathbf{r}')\mathcal{T}_3\tilde{\Psi}(\mathbf{r}')], \quad (6)$$

$$\tilde{H}_{\rm ei} = \frac{1}{2}\int d\mathbf{r}\, \tilde{\Psi}^\dagger(\mathbf{r}) V(\mathbf{r}) \mathcal{T}_3 \tilde{\Psi}(\mathbf{r}), \quad (7)$$

respectively, in which $\mathcal{T}_3 = \mathrm{diag}\{1,1,-1,-1\}$. Finally, it is addressed that in this Hamiltonian [Eqs. (5)–(7)], there exists similar gauge structure as the one in the s-wave superconductor [Eqs. (7)–(9) in Part I [1]].

B. Optical Bloch equations

In this section, we generalize the optical Bloch equations in the s-wave superconducting QWs to the ones in the $(s+p)$-wave situation. Here, in the $\mathbf{p}_s$ gauge, the optical Bloch equations in the homogeneous situation read as

$$\begin{aligned} &\frac{\partial \rho_{\mathbf{k}}}{\partial T} + i\left[\left(\frac{\mathbf{k}^2}{2m^*} - \Phi\right)\mathcal{T}_3 + h_{\mathbf{k}}^{\rm soc}, \rho_{\mathbf{k}}\right] + \frac{1}{2}\left\{\frac{\partial \mathbf{p}_s}{\partial T}\mathcal{T}_3, \frac{\partial \rho_{\mathbf{k}}}{\partial \mathbf{k}}\right\} \\ &+ i\left[\begin{pmatrix} 0 & -\alpha\mathbf{p}_s^x & 0 & 0 \\ -\alpha\mathbf{p}_s^x & 0 & 0 & 0 \\ 0 & 0 & 0 & \alpha\mathbf{p}_s^x \\ 0 & 0 & \alpha\mathbf{p}_s^x & 0 \end{pmatrix}, \rho_{\mathbf{k}}^{\rm off}\right] + i\left[\frac{\mathbf{p}_s^2}{2m^*}\mathcal{T}_3, \rho_{\mathbf{k}}\right] + i\left[\begin{pmatrix} 0 & 0 & \Delta_p e^{i\phi_{\mathbf{k}}} & \Delta_s \\ 0 & 0 & -\Delta_s & -\Delta_p e^{-i\phi_{\mathbf{k}}} \\ \Delta_p e^{-i\phi_{\mathbf{k}}} & -\Delta_s & 0 & 0 \\ \Delta_s & -\Delta_p e^{i\phi_{\mathbf{k}}} & 0 & 0 \end{pmatrix}, \rho_{\mathbf{k}}\right] \\ &= \left.\frac{\partial \rho_{\mathbf{k}}}{\partial t}\right|_{\rm HF} + \left.\frac{\partial \rho_{\mathbf{k}}}{\partial t}\right|_{\rm scat}. \end{aligned} \quad (8)$$

The details of the derivation have been outlined in Part I [1]. In Eq. (8), $\rho_{\mathbf{k}}$ is the 4×4 density matrix in the Nambu $\otimes$ spin space [24]; $\Phi = \mu - \mu_{\rm eff}$; $h_{\mathbf{k}}^{\rm soc} = -\alpha k_x \tau_0 \otimes \sigma_x + \alpha k_y \tau_3 \otimes \sigma_y$ represents the SOC Hamiltonian in the Nambu $\otimes$ spin space; $\rho_{\mathbf{k}}^{\rm off} = \frac{1}{2}(\rho_{\mathbf{k}} - \mathcal{T}_3\rho_{\mathbf{k}}\mathcal{T}_3)$ only includes the off-diagonal blocks of the density matrix. Furthermore, in Eq. (8), in the left-hand side of the equation, the fourth term comes from the supercurrent-induced effective SOC, which can directly induce the dynamics of the Cooper-pair anomalous correlation; in the right-hand side of the equation, the Hartree-Fock (HF) and scattering terms are

written as

$$\partial_t \rho_{\mathbf{k}}|_{\rm HF} = i\sum_{\mathbf{k}'} U_{\mathbf{k}-\mathbf{k}'}[\mathcal{T}_3(\rho_{\mathbf{k}'}-\bar{\rho}_{\mathbf{k}'})\mathcal{T}_3,\rho_{\mathbf{k}}], \tag{9}$$

$$\partial_t \rho_{\mathbf{k}}|_{\rm scat} = -\pi n_i \sum_{\mathbf{k}'}\sum_{\eta_1,\eta_2=1}^{4} |V_{\mathbf{k}-\mathbf{k}'}|^2 \delta(\mathcal{E}_{\mathbf{k}'\eta_1}-\mathcal{E}_{\mathbf{k}\eta_2})\big[\mathcal{T}_3\tilde{\Gamma}_{\mathbf{k}'\eta_1}\mathcal{T}_3\tilde{\Gamma}_{\mathbf{k}\eta_2}\rho_{\mathbf{k}} - \mathcal{T}_3\rho_{\mathbf{k}'}\tilde{\Gamma}_{\mathbf{k}'\eta_1}\mathcal{T}_3\tilde{\Gamma}_{\mathbf{k}\eta_2} + \text{H.c.}\big]. \tag{10}$$

Specifically, in Eq. (9), $\bar{\rho}_{\mathbf{k}}$ is the density matrix in the equilibrium state [33]. In Eq. (10), $\mathcal{E}_{\mathbf{k}1}=E^+_{\mathbf{k}}$, $\mathcal{E}_{\mathbf{k}2}=E^-_{\mathbf{k}}$, $\mathcal{E}_{\mathbf{k}3}=-E^+_{\mathbf{k}}$, and $\mathcal{E}_{\mathbf{k}4}=-E^-_{\mathbf{k}}$, where $E^\pm_{\mathbf{k}}=\sqrt{(\varepsilon^\pm_{\mathbf{k}}-\mu)^2+\Delta^2_\pm}$ with $\varepsilon^\pm_{\mathbf{k}}=\mathbf{k}^2/(2m^*)\pm\alpha k$ and $\Delta_\pm=|\Delta_s\pm\Delta_p|$. The projection operators $\tilde{\Gamma}_{\mathbf{k}\eta}=\tilde{\mathcal{U}}_{\mathbf{k}}\tilde{Q}_{\mathbf{k}\eta}\tilde{\mathcal{U}}^\dagger_{\mathbf{k}}$ with $\tilde{Q}_{\mathbf{k}1}=\text{diag}(1,0,0,0)$, $\tilde{Q}_{\mathbf{k}2}=\text{diag}(0,1,0,0)$, $\tilde{Q}_{\mathbf{k}3}=\text{diag}(0,0,1,0)$, and $\tilde{Q}_{\mathbf{k}4}=\text{diag}(0,0,0,1)$ being the projection operators in the quasiparticle space. Here, $\tilde{\mathcal{U}}_{\mathbf{k}}$ is the unitary transformation matrix from the particle space to the quasiparticle one, which is written as

$$\tilde{\mathcal{U}}_{\mathbf{k}}=\frac{\sqrt{2}}{2}\begin{pmatrix} u^+_{\mathbf{k}}e^{-i\phi_{\mathbf{k}}} & -u^+_{\mathbf{k}} & v^+_{\mathbf{k}} & v^+_{\mathbf{k}}e^{-i\phi_{\mathbf{k}}} \\ -u^-_{\mathbf{k}} & -u^-_{\mathbf{k}}e^{i\phi_{\mathbf{k}}} & v^-_{\mathbf{k}}e^{i\phi_{\mathbf{k}}} & -v^-_{\mathbf{k}} \\ v^+_{\mathbf{k}} & -v^+_{\mathbf{k}}e^{i\phi_{\mathbf{k}}} & -u^+_{\mathbf{k}}e^{i\phi_{\mathbf{k}}} & -u^+_{\mathbf{k}} \\ -v^-_{\mathbf{k}}e^{-i\phi_{\mathbf{k}}} & -v^-_{\mathbf{k}} & -u^-_{\mathbf{k}} & u^-_{\mathbf{k}}e^{-i\phi_{\mathbf{k}}} \end{pmatrix}. \tag{11}$$

In Eq. (11), $u^\pm_{\mathbf{k}}=\sqrt{1/2+\zeta^\pm_{\mathbf{k}}/(2E^\pm_{\mathbf{k}})}$ and $v^\pm_{\mathbf{k}}=\sqrt{1/2-\zeta^\pm_{\mathbf{k}}/(2E^\pm_{\mathbf{k}})}$ with $\zeta^\pm_{\mathbf{k}}=\varepsilon^\pm_{\mathbf{k}}-\mu$.

Finally, it is addressed that in Eq. (8), $\mu_{\rm eff}$ in Φ is unspecified, which can also be determined by the charge-neutrality condition from the self-consistent equation [38–45]

$$N_0=\frac{1}{2}\sum_{\mathbf{k}}\left\{2-\frac{\varepsilon^+_{\mathbf{k}}-\Phi}{\sqrt{(\varepsilon^+_{\mathbf{k}}-\Phi)^2+\Delta^2_+}}-\frac{\varepsilon^-_{\mathbf{k}}-\Phi}{\sqrt{(\varepsilon^-_{\mathbf{k}}-\Phi)^2+\Delta^2_-}}+\text{Tr}\left[\tilde{\mathcal{U}}_{\mathbf{k}}\left(\rho^h_{\mathbf{k}}-\frac{1-\mathcal{T}_3}{2}\right)\tilde{\mathcal{U}}^\dagger_{\mathbf{k}}\mathcal{T}_3\right]\right\}. \tag{12}$$

Here, N_0 is the electron density in the QWs, and $\rho^h_{\mathbf{k}}=\tilde{\mathcal{U}}^\dagger_{\mathbf{k}}\rho_{\mathbf{k}}\tilde{\mathcal{U}}_{\mathbf{k}}$ is the density matrix in the quasiparticle space. In the numerical calculation below, $\mathbf{p}_s$ takes the same form as the one in Eq. (31) in Part I [1].

III. NUMERICAL RESULTS

In this section, we present the numerical results by solving the optical Bloch equations [Eqs. (8) and (12)] in the specific material InSb (100) QWs in proximity to an s-wave superconductor. Specifically, we focus on the properties related to the spin dynamics of triplet Cooper pairs (Sec. III A). The features in the Higgs-mode excitation and charge-imbalance dynamics are also addressed (Sec. III B). All parameters used in our computation are listed in Table I [46,47].

In our computation, the electron density is chosen to be $n_e \leqslant 3N_0$. With this density, electrons mainly populate at the lower branch of the energy band ($\varepsilon^-_{\mathbf{k}}$ band), as shown in Fig. 1 by the red solid curve [24]. In this situation, one sees in Fig. 1 that the Fermi "sphere" (the blue region) is in the shape of an annulus with the inner and outer Fermi surfaces represented by the yellow and black circles. Then, some approximations can be made for the scattering term [Eq. (10)] to reduce the computation complication [48]. On one hand, with $\mu \lesssim 0$ at low temperature, the scattering between $\varepsilon^+_{\mathbf{k}}$ and $\varepsilon^-_{\mathbf{k}}$ bands contributes marginally to the scattering process; on the other hand, the scattering between the inner and outer Fermi surfaces can be neglected because, in this process, large momentum magnitude needs to be changed [48].

TABLE I. Parameters used in the computation for InSb (100) QWs in proximity to an s-wave superconductor [46,47].

m^*/m_0	0.015	N_0 (cm^{-2})	8×10^{10}
κ_0	16.8	γ_D (eV Å^3)	389
T_e (K)	5	a (nm)	3
Δ_p (meV)	0.05	σ_t (ps)	4

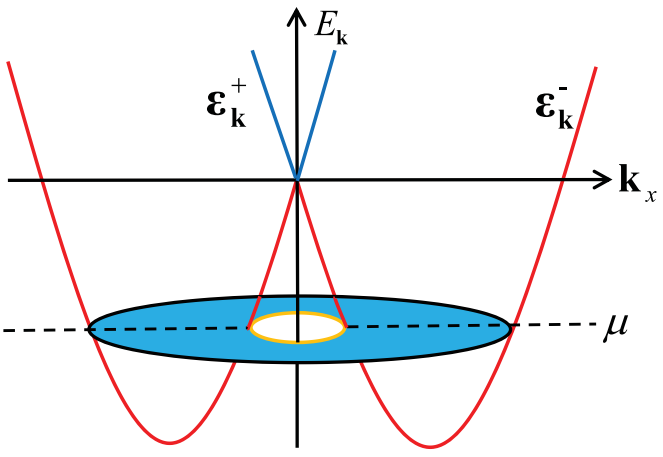

FIG. 1. Schematic of the band structures of $\varepsilon^+_{\mathbf{k}}$ and $\varepsilon^-_{\mathbf{k}}$ bands, shown by the blue and red solid curves, respectively. The dashed line labeled by μ corresponds to the chemical potential, with which only the lower band is efficiently populated. In this situation, one sees that the Fermi "sphere" (the blue region) is in the shape of an annulus with the inner and outer Fermi surfaces represented by the yellow and black circles.

A. Optical excitation of spin polarization of Cooper pairs

In our previous work [33], it has been revealed that in the InSb (100) QWs in proximity to an s-wave superconductor, due to the Dresselhaus SOC, the spin polarization of electrons in the momentum space is parallel to the effective magnetic field $\mathbf{\Omega}(\mathbf{k})$ due to the SOC in the equilibrium state. This feature is all the same as the one in the normal state [24,48]. In the *normal* state, it has been well understood that when there exists electrical field, with the drift of electron states due to the applied field, this parallel relation is broken and hence the effective magnetic field $\mathbf{\Omega}(\mathbf{k})$ can induce the momentum-dependent out-of-plane spin polarization, which accounts for the spin current of electrons [48]. Moreover, the center-of-mass momentum driven by the electrical field contributes to the effective magnetic field, which tends to polarize the electron states along this effective magnetic field [2,3,5,6]. In the superconducting state in our configuration, we show that both the spin polarization and spin current can be induced by the optical field, which oscillate with the same frequency of the optical field. Nevertheless, with our computation parameters, we find that the order parameters have little influence on the optical generations of the spin polarization and spin current. The details are presented in the Appendix.

Furthermore, in the superconducting InSb (100) QWs, we have revealed that there exists p-wave triplet Cooper pairing in $(p_x \pm ip_y)$ type [33]. With the frequency- and momentum-dependent [7,14–16] Cooper pairing written as $[f_s(\mathbf{k},\omega) + \mathbf{f}(\mathbf{k},\omega)\cdot\boldsymbol{\sigma}]i\sigma_y$, it can be further shown that the $\mathbf{f}$ vector of the triplet Cooper pairing is also parallel to the effective magnetic field $\mathbf{\Omega}(\mathbf{k})$ due to the SOC [33]. By analogy with the optical generation of the spin polarization addressed above, one expects that the $\mathbf{f}$ vector can also be controlled by the optical field. Actually, very recently, Tkachov indeed showed that in noncentrosymmetric superconductors, the driven center-of-mass momentum $\mathbf{q}$ of the Cooper pairs can induce the nonunitary triplet pairing, which contributes to the spin polarization of the triplet Cooper pairs [16]. Specifically, with the spin polarization of Cooper pairs $\mathbf{S}_{\mathbf{k}}^{\mathrm{CP}}$ described by $i\mathbf{f}(\mathbf{k},\omega=0)\times\mathbf{f}^*(\mathbf{k},\omega=0)$, Tkachov showed that with small superfluid velocity with the triplet Cooper pairing derived, the Cooper-pair spin polarization (refer to Ref. [16] for the detailed derivation)

$$\mathbf{S}_{\mathbf{k}}^{\mathrm{CP}} = i\mathbf{f}(\mathbf{k},\omega=0)\times\mathbf{f}^*(\mathbf{k},\omega=0) \propto \mathbf{\Omega}_{\mathbf{k}} \times[\mathbf{\Omega}_{\mathbf{k}}\times(\mathbf{q}\cdot\partial_{\mathbf{k}})\mathbf{\Omega}_{\mathbf{k}}]. \quad (13)$$

Actually, before the concrete calculation, the feature of Cooper-pair spin polarization in (100) InSb QWs can be roughly conjectured based on Eq. (13). Here, for the Dresselhaus SOC in the Rashba type, i.e., Eq. (4), with the center-of-mass momentum $\mathbf{q} = q_x\hat{\mathbf{x}}$, we conjecture from Eq. (13)

$$\mathbf{S}_{\mathbf{k}}^{\mathrm{CP}} \propto \mathbf{\Omega}_{\mathbf{k}}\times[\mathbf{\Omega}_{\mathbf{k}}\times(\mathbf{q}\cdot\partial_{\mathbf{k}})\mathbf{\Omega}_{\mathbf{k}}] = q_x k_y^2\hat{\mathbf{x}} + q_x k_x k_y\hat{\mathbf{y}}. \quad (14)$$

This indicates that the $\hat{\mathbf{x}}$ component ($\hat{\mathbf{y}}$ component) of the Cooper-pair spin polarization is even (odd) in momentum, which is proportional to k_y^2 ($k_x k_y$). Then, the *total* Cooper-pair spin polarization, which is in sum of the momentum, is along the $\hat{\mathbf{x}}$ direction.

In our framework, in the density matrix, the information about the frequency has been integrated [Eq. (19) in Part I [1]], in which the Cooper pairing is integrated to be the anomalous correlation [13,24,33]. Actually, it is reasonable to define

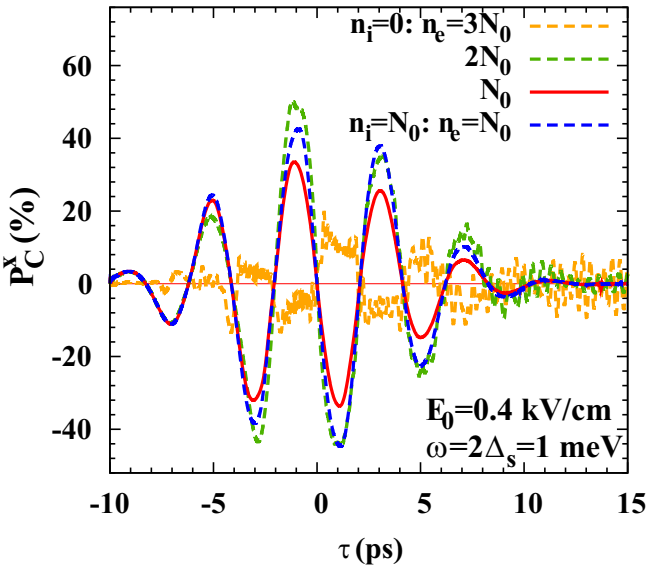

FIG. 2. Temporal evolutions of the $\hat{\mathbf{x}}$ component of the total Cooper-pair spin polarization $\mathbf{P}_{\mathrm{C}}^x$ with different electron densities $n_e = 3N_0$ (yellow dashed curve), $2N_0$ (green chain curve), and N_0 [red solid (blue dotted) curve in the absence (presence) of the impurity]. $E_0 = 0.4$ kV/cm. The blue dotted curve denotes the total Cooper-pair spin polarization in the presence of the impurity with $n_i = N_0$.

the Cooper-pair spin polarization by using the anomalous correlation but not Cooper pairing at zero frequency [16]. Microscopically, the Cooper-pair spin polarization is calculated by the wave function of the triplet Cooper pairs [Eq. (2)], which does not depend on the relative temporal coordinate (refer to Ref. [13]). Furthermore, the Fourier components of the Cooper-pair wave function are exactly the *anomalous correlation* [13], which can be directly calculated by the optical Bloch equations. Here, the anomalous correlation of the Cooper pairs is conveniently expressed as

$$\begin{pmatrix}\rho_{13}(\mathbf{k}) & \rho_{14}(\mathbf{k})\\ \rho_{23}(\mathbf{k}) & \rho_{24}(\mathbf{k})\end{pmatrix} = [l_0(\mathbf{k})\sigma_0 + \mathbf{l}(\mathbf{k})\cdot\boldsymbol{\sigma}]i\sigma_y, \quad (15)$$

in which the $\mathbf{l}$ vector (l_0) describes the anomalous correlation of the triplet (singlet) Cooper pairs. Accordingly, from definition of the Cooper-pair spin polarization in Eq. (3), by using the $\mathbf{l}$ vector, the total spin polarization of the Cooper pair reads as

$$\mathbf{P}_{\mathrm{C}} = \frac{\sum_{\mathbf{k}} i\mathbf{l}(\mathbf{k})\times\mathbf{l}^*(\mathbf{k})}{\sum_{\mathbf{k}}[|\mathbf{l}_x(\mathbf{k})|^2 + |\mathbf{l}_y(\mathbf{k})|^2 + |\mathbf{l}_z(\mathbf{k})|^2]}, \quad (16)$$

in which the denominator is introduced to act as the normalization factor.

Then, the temporal evolution of $\mathbf{P}_{\mathrm{C}}$ is calculated by the optical Bloch equations, in which it is found that only the $\hat{\mathbf{x}}$ component $\mathbf{P}_{\mathrm{C}}^x$ exists, in agreement with the analysis in Eq. (14). Specifically, in Fig. 2, the temporal evolutions of $\mathbf{P}_{\mathrm{C}}^x$ are plotted with different electron densities $n_e = 3N_0$ (yellow dashed curve), $2N_0$ (green chain curve), and N_0 [red solid (blue dotted) curve in the absence (presence) of the impurity]. It is noted that for these three electron densities, the chemical potentials are about 4.2, -9.9, and -15.6 meV, respectively, which are larger than the minimal value of the energy spectra $-m^*\alpha^2/2 \approx -17.9$ meV [33]. In Fig. 2, it can

be seen that in the impurity-free situation, when $n_e = 2N_0$ and N_0, the total spin polarizations of the Cooper pairs are significant, which oscillate with the frequency of the optical field. Whereas when $n_e = 3N_0$, corresponding to a positive chemical potential, the total Cooper-pair spin polarization is efficiently suppressed, whose oscillation does not show a particular pattern. This reveals that the low electron density with *single-band population* is in favor of the realization of significant Cooper-pair total spin polarization. This is in contrast to the optical excitation of the electron spin polarization, which is less influenced by the electron density (refer to the Appendix). Finally, we also calculate the total Cooper-pair spin polarization with the impurity density $n_i = N_0$, which is presented by the blue dotted curve in Fig. 2. One finds that the impurity can even enhance the optical excitation of the total Cooper-pair spin polarization.

To further reveal the dynamical features of $\mathbf{P}_C$ from the microscopic viewpoint, we calculate the momentum distribution of the Cooper-pair spin vector $\mathbf{n}(\mathbf{k}) \equiv i\mathbf{l}(\mathbf{k}) \times \mathbf{l}^*(\mathbf{k})$ in the dynamical evolution. When $n_e = N_0$ in the impurity-free situation, at a particular time $\tau = 0.5$ ps with $\mathbf{p}_s^x \approx -0.4k_F < 0$ ($k_F = \sqrt{2\pi N_0}$), the $\hat{\mathbf{x}}$ and $\hat{\mathbf{y}}$ components of $\mathbf{n}(\mathbf{k})$ in the momentum space are plotted in Figs. 3(a) and 3(b), respectively. With this electron density $n_e = N_0$, the Fermi "sphere" is in the shape of an annulus with the inner and outer Fermi surfaces (refer to Fig. 1). It can be seen that $\mathbf{n}(\mathbf{k})$ is significant only around the inner and outer Fermi surfaces [24,33]. Moreover, one finds that $\mathbf{n}_x(\mathbf{k}) \propto -k_y^2$ and $\mathbf{n}_y(\mathbf{k}) \propto -k_x k_y$ in both the inner and outer Fermi surfaces, in agreement with Eq. (14). Thus, only $\mathbf{n}_x(\mathbf{k})$ contributes to the total Cooper-pair spin polarization after the sum of momentum. Furthermore, a specific feature is found by comparing the Cooper-pair spin vectors in the inner and outer Fermi surfaces. It is intriguing to observe that both $\mathbf{n}_x(\mathbf{k})$ and $\mathbf{n}_y(\mathbf{k})$ are larger in the inner Fermi surface than those in the outer one. These numerical results can be understood from the analytical analysis in the following.

It is convenient to set up simplified kinetic equations for l_0 and $\mathbf{l}$ vector from the optical Bloch equations [Eq. (8)], which can be used to analyze the dynamics of Cooper pairing directly. Moreover, from the simplified kinetic equations, the kinetic equations for the Cooper-pair spin vectors can be obtained. Specifically, with the third, fifth, and sixth terms in the left-hand side and the HF term in the right-hand side of Eq. (8) neglected, (which have been checked to be unimportant in the excitation of Cooper-pair spin polarization by the numerical calculations), the kinetic equations for l_0 and $\mathbf{l}$ vector become

$$\partial_T(l_0 + \mathbf{l}\cdot\boldsymbol{\sigma}) + i\{\zeta_{\mathbf{k}} - \alpha k_x\sigma_x + \alpha k_y\sigma_y, l_0 + \mathbf{l}\cdot\boldsymbol{\sigma}\} + i\big[-\alpha \mathbf{p}_s^x\sigma_x, l_0 + \mathbf{l}\cdot\boldsymbol{\sigma}\big] = 0. \tag{17}$$

In the matrix form,

$$\partial_T \begin{pmatrix} l_{\mathbf{k}}^0 \\ \mathbf{l}_{\mathbf{k}}^x \\ \mathbf{l}_{\mathbf{k}}^y \\ \mathbf{l}_{\mathbf{k}}^z \end{pmatrix} + 2i \begin{pmatrix} \zeta_{\mathbf{k}} & -\alpha k_x & \alpha k_y & 0 \\ -\alpha k_x & \zeta_{\mathbf{k}} & 0 & 0 \\ \alpha k_y & 0 & \zeta_{\mathbf{k}} & i\alpha \mathbf{p}_s^x \\ 0 & 0 & -i\alpha \mathbf{p}_s^x & \zeta_{\mathbf{k}} \end{pmatrix} \begin{pmatrix} l_{\mathbf{k}}^0 \\ \mathbf{l}_{\mathbf{k}}^x \\ \mathbf{l}_{\mathbf{k}}^y \\ \mathbf{l}_{\mathbf{k}}^z \end{pmatrix} = 0. \tag{18}$$

In Eq. (18), one finds that l_0 is coupled to the $\mathbf{l}$ vector due to the SOC. It is noted that in the equilibrium state, the $\mathbf{l}$ vector of the triplet Cooper correlation is parallel to the effective magnetic field $\boldsymbol{\Omega}(\mathbf{k})$ due to the SOC in the momentum space.

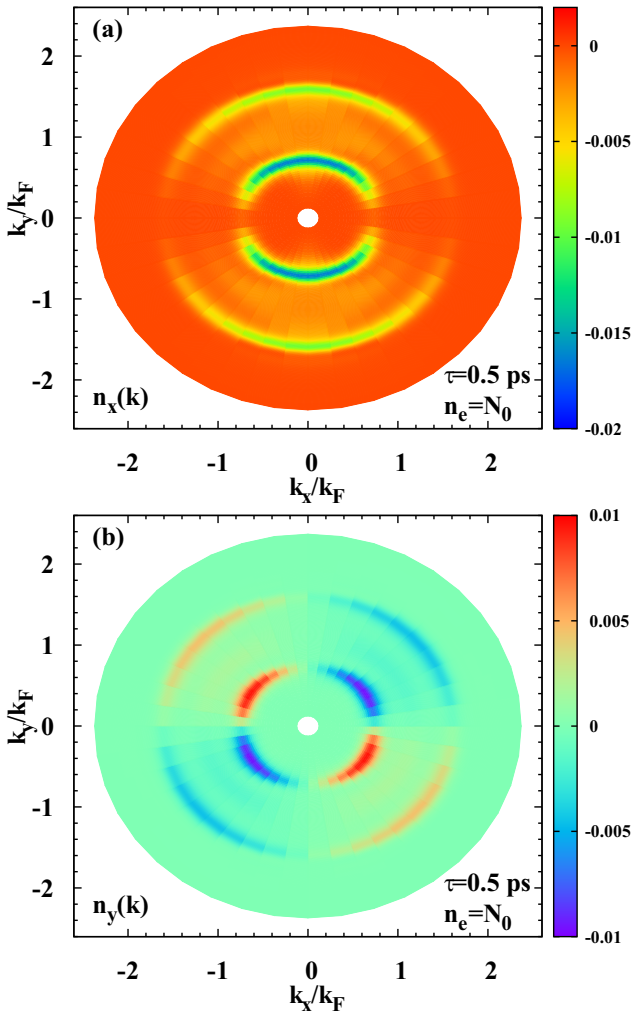

FIG. 3. Momentum distributions of the Cooper-pair spin vectors $\mathbf{n}_x(\mathbf{k})$ (a) and $\mathbf{n}_y(\mathbf{k})$ (b) at $\tau = 0.5$ ps when $n_e = N_0$ and $n_i = 0$. $E_0 = 0.4$ kV/cm. At this particular time $\tau = 0.5$ ps, $\mathbf{p}_s^x \approx -0.4k_F < 0$ with $k_F = \sqrt{2\pi N_0}$. In the figures, it can be seen that $\mathbf{n}_x(\mathbf{k}) \propto -k_y^2$ and $\mathbf{n}_y(\mathbf{k}) \propto -k_x k_y$ in both the inner and outer Fermi surfaces, in agreement with Eq. (14). One further observes that both $\mathbf{n}_x(\mathbf{k})$ and $\mathbf{n}_y(\mathbf{k})$ are larger in the inner Fermi surface than the those in the outer Fermi one.

When the optical field with in-plane vector potential is applied to the superconducting system, the superconducting velocity is induced, which directly contributes to the effective SOC, i.e., $\pm i\alpha \mathbf{p}_s^x$, in Eq. (18). This effective SOC can cause the precession of the $\mathbf{l}$ vectors, with the component perpendicular to $\boldsymbol{\Omega}(\mathbf{k})$ induced. Thus, from the definition $\mathbf{n}(\mathbf{k}) = i\mathbf{l}(\mathbf{k}) \times \mathbf{l}^*(\mathbf{k})$ [16], the Cooper-pair spin polarization $\mathbf{n}(\mathbf{k})$ is expected.

To make this point more concrete, from Eq. (18), the kinetic equations for the $\mathbf{n}$ vector can be derived, written as

$$\partial_T^2 \mathbf{n}_x + 4\alpha^2 k_y(k_x \mathbf{n}_y + k_y \mathbf{n}_x) + 4\alpha^2 k_y \mathbf{p}_s^x(\mathbf{l}_y^* l_0 + \mathbf{l}_y l_0^*) = 0, \tag{19}$$

$$\partial_T \mathbf{n}_y = (k_x/k_y)\partial_T \mathbf{n}_x + 2\alpha \mathbf{p}_s^x \mathbf{n}_z, \tag{20}$$

$$\partial_T^2 \mathbf{n}_z + 4\alpha^2 k^2 \mathbf{n}_z + 2\alpha \mathbf{p}_s^x \partial_T \mathbf{n}_y + 4\alpha^2 k_x \mathbf{p}_s^x(\mathbf{l}_z^* l_0 + \mathbf{l}_z l_0^*) = 0. \tag{21}$$

From Eqs. (19)–(21), it is concluded that $\mathbf{n}_x \propto \mathbf{p}_s^x$, $\mathbf{n}_y \propto \mathbf{p}_s^x$, and $\mathbf{n}_z \propto (\mathbf{p}_s^x)^2$. This is because in the equilibrium state, $\bar{\mathbf{l}}_z = 0$ ("bar" labels the equilibrium state), whose first-order deviation is proportional to $\mathbf{p}_s^x$. By only keeping the quantities in the first order of $\mathbf{p}_s^x$, one obtains from Eq. (20) that

$$k_y \mathbf{n}_y = k_x \mathbf{n}_x, \tag{22}$$

which satisfies the numerical results presented in Figs. 3(a) and 3(b). Thus, from Eq. (19), one obtains

$$\partial_T^2 \mathbf{n}_x + 4\alpha^2 k^2 \mathbf{n}_x + 8\alpha^2 k_y \mathbf{p}_s^x \bar{\mathbf{l}}_y \bar{l}_0 = 0, \tag{23}$$

whose solution reads as

$$\mathbf{n}_x(\mathbf{k}) \approx \frac{8\alpha^2 k_y^2 \bar{\mathbf{l}}_y \bar{l}_0}{\omega^2 - 4\alpha^2 k^2} \mathbf{p}_s^x. \tag{24}$$

Here, $\bar{l}_0(\mathbf{k})$ and $\bar{\mathbf{l}}_y(\mathbf{k})$ in the equilibrium state are [24,33]

$$\bar{l}_0 = u_{\mathbf{k}}^+ v_{\mathbf{k}}^+ [2 f_0(E_{\mathbf{k}}^+) - 1] + u_{\mathbf{k}}^- v_{\mathbf{k}}^- [2 f_0(E_{\mathbf{k}}^-) - 1], \tag{25}$$

$$\bar{\mathbf{l}}_y = \frac{k_y}{k} \{u_{\mathbf{k}}^+ v_{\mathbf{k}}^+ [2 f_0(E_{\mathbf{k}}^+) - 1] - u_{\mathbf{k}}^- v_{\mathbf{k}}^- [2 f_0(E_{\mathbf{k}}^-) - 1]\}. \tag{26}$$

It is noted that when ω tends to zero, Eq. (24) directly recovers the static results in the work of Tkachov [16]. Furthermore, Eq. (24) also describes the dynamical situation especially at the high frequency. Moreover, it is expected that the Cooper-pair spin polarization can be resonantly excited for particular momenta around $k^* \equiv \omega/(2\alpha)$. Nevertheless, this resonance is pronounced only when $k^* \approx k_F$, at which the anomalous correlations in the equilibrium states $\bar{l}_0(\mathbf{k})$ and $\bar{\mathbf{l}}(\mathbf{k})$ are significant.

The features for the dynamics of Cooper-pair spin polarization revealed in the numerical calculation can be understood based on Eq. (24). Specifically, from Eqs. (22) and (24)–(26), one obtains that $\mathbf{n}_x(\mathbf{k}) \propto k_y^2 \mathbf{p}_s^x$ and $\mathbf{n}_y(\mathbf{k}) \propto k_x k_y \mathbf{p}_s^x$, confirming the conjecture in Eq. (14). Furthermore, it is observed that in Eq. (26), the contributions of the anomalous correlation from the lower and upper bands are opposite, which is relatively large in the situation with *single-band population* [33] (refer to Fig. 2). Thus, the induced total Cooper-pair polarization is significant when only the lower band is populated. It is noted when $n_e \geqslant N_0$, $\omega \ll \alpha k$. Thus,

$$\mathbf{n}_x(\mathbf{k}) \approx -2(k_y/k^2) \bar{\mathbf{l}}_y \bar{l}_0 \mathbf{p}_s^x, \tag{27}$$

which is inversely proportional to the momentum. This relation naturally explains the calculated results that the induced Cooper-pair spin vector is larger in the inner Fermi surface than the one in the outer Fermi surface (refer to Fig. 3). Finally, it is addressed that from Eq. (24), it is obtained that the Cooper-pair spin polarization is stabilized by the superconducting momentum.

B. Higgs mode and charge imbalance

In this section, we consider the dynamics of the Higgs mode and charge imbalance excited by the THz pulses in the $(s+p)$-wave superconducting InSb (100) QWs. In this configuration, although there exists strong SOC, most features for the dynamics of the Higgs mode and charge imbalance are revealed to be similar to those in the s-wave one (refer to Part I [1]). Nevertheless, a novel regime with $|\mathbf{p}_s|$ larger than the Fermi momentum can be realized without destroying the superconductivity. One notes that the regime with $|\mathbf{p}_s|$ larger than the Fermi momentum is hard to be realized in the QWs with a single Fermi surface, e.g., the s-wave superconducting GaAs QWs considered in Part I [1], in which the superconductivity can be destroyed when $|\mathbf{p}_s| \gtrsim k_F$. Nevertheless, with typical electron densities $n_e \lesssim 3N_0$, in InSb (100) QWs, the specific band structure results in two Fermi surfaces due to the strong SOC, which are labeled by the yellow and black circles in Fig. 1. It is observed that the Fermi momentum of the inner Fermi surface (inner Fermi momentum) can be much smaller than one of the outer Fermi surface (outer Fermi momentum). Thus, in InSb QWs, the superconducting momentum can be tuned to be larger than the inner Fermi momentum but smaller than the outer one, but without destroying the superconductivity.

Particularly, compared to the situation in the s-wave superconducting GaAs QWs, when $|\mathbf{p}_s|$ is tuned to be larger than the inner Fermi momentum in InSb QWs, some new features in the excitation of the Higgs mode and creation of the charge imbalance are expected. For the excitation of the Higgs mode, in GaAs QWs, we have shown that the pump effect plays a marginal role (refer to Part I [1]). Nevertheless, it is estimated that the pump effect influences the excitation of the Higgs mode as long as $|\mathbf{p}_s|$ is larger than the Fermi momentum. Accordingly, with $|\mathbf{p}_s|$ larger than the inner Fermi momentum in InSb (100) QWs, the pump of the quasiparticles around the inner Fermi surface is now expected. For the creation of the charge imbalance, in GaAs QWs, we have found that the pump effect still has significant contribution (refer to Part I [1]). Furthermore, it is revealed that the charge imbalance is contributed by the pump and drive effects separately, through influencing the quasiparticle correlation and quasiparticle population, respectively (refer to Part I [1]). This fact indicates that in GaAs QWs, the system still lies in the "linear" regime without any interplay between the pump and drive effects. Nevertheless, when $|\mathbf{p}_s|$ is tuned to be larger than the inner Fermi momentum in InSb QWs, the interplay between the pump and drive effects is expected.

1. Higgs mode

We first focus on the Higgs mode. As with the electron densities we considered ($n_e \leqslant 3N_0$), the triplet order parameter and its fluctuation are much smaller than the singlet one [24], here we focus on the Higgs mode contributed by the singlet order parameter $|\delta\Delta_s|$. In Fig. 4, the temporal evolutions of the Higgs mode $|\delta\Delta_s|$ are plotted with different optical-field frequencies $\omega = 2\Delta_s$ (green dashed curve) and $4\Delta_s$ (red solid curve) when $n_e = N_0$. The electrical-field strength is taken to be relatively large $E_0 = 0.4$ kV/cm, with which the peak value of $\mathbf{p}_s$ is about $0.6\tilde{k}_F$ ($0.3\tilde{k}_F$) when $\omega = 2\Delta_s$ ($\omega = 4\Delta_s$). Here, $\tilde{k}_F = \sqrt{2\pi N_0}$. With this electric field, the peak value of $\eta \approx 2$ meV when $\omega = 2\Delta_s$ is larger than $2\Delta_s = 1$ meV, indicating that the system lies in the strong-pump regime. It can be seen in Fig. 4 that the Higgs modes $|\delta\Delta_s|$ oscillate with twice the frequency of the optical field and plateaus appear after the optical pulse. These features are similar to the ones in the s-wave superconducting QWs.

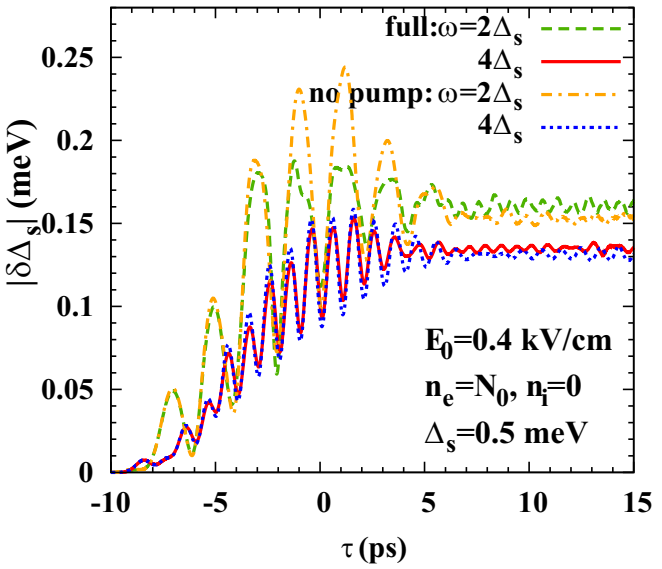

FIG. 4. Temporal evolutions of the Higgs mode for the singlet order parameter $|\delta\Delta_s|$ with different frequencies $\omega = 2\Delta_s$ (green dashed curve) and $4\Delta_s$ (red solid curve) when $n_e = N_0$ and $n_i = 0$. $E_0 = 0.4$ kV/cm. When the pump effect is neglected, $|\delta\Delta_s|$ are plotted for $\omega = 2\Delta_s$ (yellow chain curve) and $4\Delta_s$ (blue dotted curve). By comparing the green dashed (red solid) curve with the yellow chain (blue dotted) curve, one finds that when $\omega = 2\Delta_s$ ($\omega = 4\Delta_s$), the pump effect can have significant (marginal) role in the excitation of the Higgs mode.

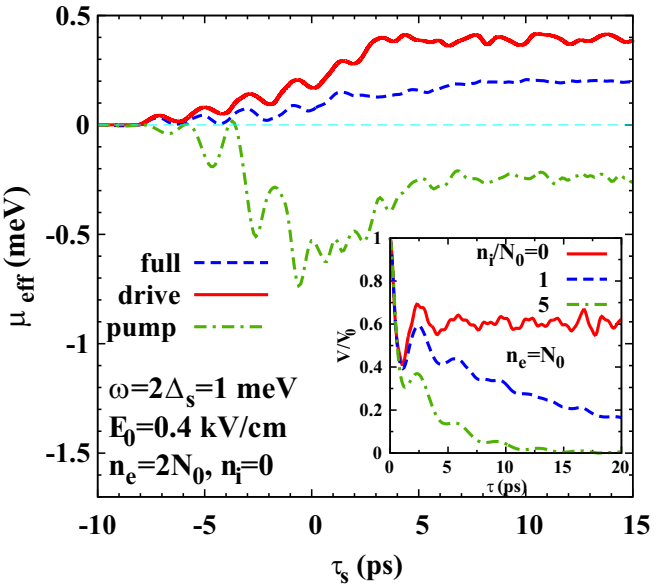

FIG. 5. Temporal evolutions of the effective chemical potential in the free situation. The electron density $n_e = 2N_0$ and $\omega = 2\Delta_s \approx 1.15$ THz. The electric field strength is relatively large with $E_0 = 0.4$ kV/cm, with which the system lies in the strong-pump regime. In the figure, the blue dashed curve denotes the full calculation with both the drive and pump effects included, whereas the red solid (green chain) curve represents the calculated results with only the drive (pump) effect retained. In the inset, the temporal evolution of the charge imbalance is presented with $n_e = N_0$ with different impurity densities $n_i = 0$ (the red solid curve), $n_i = N_0$ (the blue dashed curve), and $n_i = 5N_0$ (the green chain curve), respectively.

However, it is observed that the pump effect can have significant contribution to the excitation of the Higgs mode when $\omega = 2\Delta_s$, in contrast to the situation in the s-wave superconducting QWs (refer to Part I [1]). It is shown in Fig. 4 that with the pump effect neglected in the calculation, when $\omega = 2\Delta_s$, the yellow chain curve is markedly different from the green dashed curve; nevertheless, when $\omega = 4\Delta_s$, the blue dotted curve still almost coincides with the red solid one. These can be understood as follows. It is noted that when $n_e = N_0$ here, the Fermi momentum of the inner (outer) Fermi surface $k_F^< \approx 0.5\tilde{k}_F$ ($k_F^> \approx 1.4\tilde{k}_F$). Thus, when $\omega = 2\Delta_s$, $|\mathbf{p}_s| \lesssim 0.6\tilde{k}_F$ can be comparable to the Fermi momentum of the inner Fermi surface, indicating that the system lies in the regime with $|\mathbf{p}_s| \gtrsim k_F^<$. In this regime, it has been estimated that the pump effect can survive from the Pauli blocking due to the drive effect and hence contribute to the excitation of the Higgs mode (refer to Part I [1]). Furthermore, by comparing the yellow chain and green dashed curves, one observes that the pump effect actually suppresses, rather enhances, the excitation of the Higgs mode.

2. *Charge imbalance*

Then, we analyze the optical excitation of the charge imbalance. The temporal evolutions of the effective chemical potential are shown in Fig. 5 in the free situation. In the calculation, the electron density $n_e = 2N_0$ and $\omega = 2\Delta_s = 1$ meV. The electric-field strength is relatively large with $E_0 = 0.4$ kV/cm, with which the system lies not only in the strong-pump regime, but also in the regime with $|\mathbf{p}_s| \gtrsim k_F^<$. In Fig. 5, the blue dashed curve denotes the full calculation with both the drive and pump effects included, whereas the red solid (green chain) curve represents the calculated results with only the drive (pump) effect retained. It can be seen that the effective chemical potential is always positive, and no longer equals to the sum of the ones contributed by the drive and pump effects separately. This is in contrast to the features revealed in the s-wave superconducting GaAs QWs, indicating that there exists significant interplay between the pump and drive effects. Moreover, our calculated results indicate that in the competition between the pump and drive effects in the creation of the charge imbalance, the drive effect is dominant.

Finally, it is addressed that the electron-impurity scattering can still provide the charge-imbalance relaxation channel in the $(s + p)$-wave superconducting QWs, whose features are similar to the situation in the s-wave one (refer to Part I [1]). This can be seen in the inset of the Fig. 5 that when $n_i = 0$, the normalized effective chemical potential V/V_0 does not relax to zero, represented by the red solid curve, whereas when there exists impurities, the relaxation channel for the charge imbalance can be opened, as shown by the blue dashed ($n_i = N_0$) and green chain ($n_i = 5N_0$) curves.

IV. SUMMARY

In summary, we have investigated the quasiparticle and condensate dynamics in response to the THz optical pulses in the strong spin-orbit-coupled $(s+p)$-wave superconducting semiconductor QWs. Similar to the s-wave case in Part I [1], we set up the gauge-invariant optical Bloch equations in the quasiparticle approximation via the gauge-invariant nonequilibrium Green function approach [25,26,30], with the gauge structure revealed by Nambu explicitly retained [32]. Both the dynamics of triplet and singlet superconductivity are studied in response to the THz optical pulses.

For the triplet superconductivity, we focus on the study on the optical excitation of the Cooper-pair spin polarization. By using the optical Bloch equations, the optical creation of the spin polarization for the Cooper pairs is investigated in the $(s+p)$-wave superconducting InSb (100) QWs. We predict that when the optical field with the in-plane vector potential applied, the total spin polarization of triplet Cooper pairs can be induced, which is shown to be parallel to the vector potential and oscillates with the frequency of the optical field. This can be understood as follows.

In the equilibrium state, in the InSb superconducting (100) QWs with the Dresselhaus SOC, the $\mathbf{l}$ vector of the anomalous correlation for the triplet Cooper pairs is parallel to the effective magnetic field $\mathbf{\Omega}(\mathbf{k})$ due to the SOC [33]. Here, $\mathbf{l}$ vector is defined from $[\mathbf{l}(\mathbf{k})\cdot\boldsymbol{\sigma}]i\sigma_y=\begin{pmatrix}F_{\uparrow\uparrow}(\mathbf{k}) & F_{\uparrow\downarrow}(\mathbf{k})\\ F^*_{\uparrow\downarrow}(\mathbf{k}) & F_{\downarrow\downarrow}(\mathbf{k})\end{pmatrix}$ with $F(\mathbf{k})$ representing the Fourier components of triplet Cooper-pair wave function in spatial space [13]. When the optical field with the in-plane vector potential is applied to this superconducting system, the superconducting velocity is induced, which is shown to contribute to an effective SOC. This induced effective SOC can cause the precession of the $\mathbf{l}$ vectors, with the component perpendicular to $\mathbf{\Omega}(\mathbf{k})$ induced. Thus, the Cooper-pair spin vector can be induced by its definition $\mathbf{n}(\mathbf{k})=i\mathbf{l}(\mathbf{k})\times\mathbf{l}^*(\mathbf{k})$ [16], whose summation by momentum contributes to the total spin polarization of Cooper pairs $\mathbf{P}_C$ [Eq. (3)]. It is demonstrated that the induced Cooper-pair spin vector $\mathbf{n}(\mathbf{k})$ is inversely proportional to the momentum. Moreover, it is revealed that the Cooper-pair spin polarization is proportional to the superconducting velocity, which oscillates with the frequency of the optical field. This shows that the Cooper-pair spin polarization is directly stabilized by the superconducting momentum.

From the experimental point of view, we remark the possible experimental detection for the induction of the Cooper-pair spin polarization by the optical technique. Actually, its direct observation is not as easy as the spin polarization of electrons. Nevertheless, it was proposed by Tkachov that the Cooper-pair spin polarization can be detected by the magnetoelectric Andreev effect [16].

For the singlet superconductivity, we reveal several features in the dynamics of the Higgs mode and charge imbalance induced by the optical field in comparison with the conventional s-wave case (refer to Part I [1]). We show that with typical electron density in InSb (100) QWs, due to the strong SOC, the specific band structure results in two Fermi surfaces, including the the inner and outer ones. In this specific configuration, the superconducting momentum can be tuned to be larger than the inner Fermi momentum but smaller than the outer one. We find that in this regime, features in the dynamics of the Higgs mode and charge imbalance are revealed in comparison with the conventional s-wave case (refer to Part I [1]). Specifically, we find that in this regime, the pump effect can indeed have contribution to the excitation of the Higgs mode, which has been shown to play a negligible role in the s-wave case in Part I [1]. Moreover, in this regime, we reveal that there exists interplay between the pump and drive effects in the excitation of the charge imbalance.

ACKNOWLEDGMENTS

This work was supported by the National Natural Science Foundation of China under Grants No. 11334014 and No. 61411136001. One of the authors (T.Y.) would like to thank M. Q. Weng for helpful discussions.

APPENDIX: OPTICAL GENERATIONS OF SPIN POLARIZATION AND SPIN CURRENT

We first define the spin polarization and spin current in the $(s+p)$-wave superconducting (100) QWs. The temporal evolution of the total spin polarization of the system is calculated by [24,49]

$$\mathbf{P}\equiv(P_x,P_y,P_z)=(1/2)\sum_{\mathbf{k}}\mathrm{Tr}(\rho_{\mathbf{k}}\boldsymbol{\alpha})/n_0, \tag{A1}$$

in which

$$\boldsymbol{\alpha}=\frac{1+\tau_3}{2}\otimes\boldsymbol{\sigma}+\frac{1-\tau_3}{2}\otimes\sigma_y\boldsymbol{\sigma}\sigma_y. \tag{A2}$$

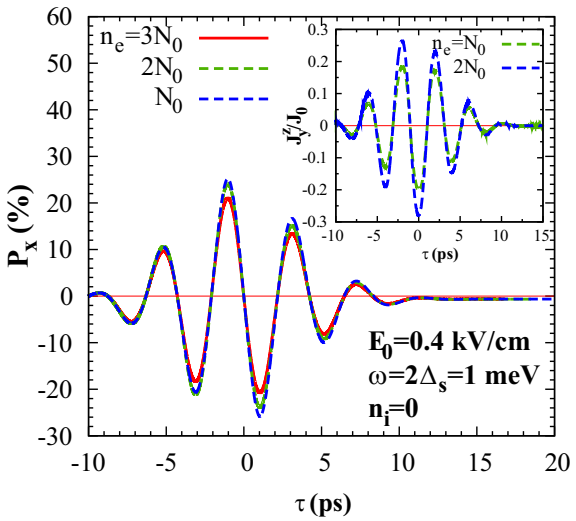

FIG. 6. Temporal evolutions of optically generated spin polarization with different electron densities $n_e=N_0$ (red solid curve), $2N_0$ (green dashed curve), and $3N_0$ (blue dashed curve). $E_0=0.4\,\mathrm{kV/cm}$. The optically generated spin polarization is along the $\hat{\mathbf{x}}$ direction, i.e., in parallel to the optically induced supercurrent, and oscillates with the same frequency of the optical field. The spin current is presented in the inset, which is calculated according to Eq. (A3). $J_0=n_ek_F(k_BT_e/E_F)$ with $k_F=\sqrt{2\pi n_e}$ and $E_F=\pi n_e/m^*$.

Then, the spin current is defined as [48,50–53]

$$\mathbf{J}^{\hat{\boldsymbol{\alpha}}}_{\hat{\mathbf{v}}} = \sum_{\mathbf{k}} \mathrm{Tr}(\{\mathbf{v},\boldsymbol{\alpha}\}\rho_{\mathbf{k}})/2. \tag{A3}$$

Here, the velocity operator is calculated by the Heisenberg equation $\hat{\mathbf{v}} = -i[\hat{\mathbf{r}}, \hat{H}_0(\mathbf{A}=0)]$ [36,54,55]. Specifically,

$$v_y = \begin{pmatrix} k_y/m^* & -i\alpha & \Delta_p f(\mathbf{k}) & 0 \\ i\alpha & k_y/m^* & 0 & -\Delta_p f^*(\mathbf{k}) \\ \Delta_p f^*(\mathbf{k}) & 0 & -k_y/m^* & i\alpha \\ 0 & -\Delta_p f(\mathbf{k}) & -i\alpha & -k_y/m^* \end{pmatrix}, \tag{A4}$$

with $f(\mathbf{k}) = (-k_x k_y + i k_x^2)/k^3$.

According to Eq. (A1), the temporal evolutions of the optically generated spin polarization are shown in Fig. 6 with different electron densities $n_e = N_0$ (red solid curve), $2N_0$ (green dashed curve), and $3N_0$ (blue dashed curve). It is shown that the optically generated spin polarization is along the $\hat{\mathbf{x}}$ direction, i.e., in parallel to the optically induced supercurrent, and oscillates with the same frequency of the optical field. This is consistent with the previous studies in the system with Rashba SOC [2,3,5]. Furthermore, the calculated results with different electron densities show that the generated spin polarization is less influenced by the electron density. In the inset of Fig. 6, the spin current is presented, which is calculated according to Eq. (A3). It is shown that the induced spin current is perpendicular to the total electrical current with the spin polarization being along the $\hat{\mathbf{z}}$ direction, oscillating with the frequency of the optical field. By noticing that the spin current is divided by $J_0 = n_e k_F (k_B T_e/E_F) \propto \sqrt{n_e}$ with $k_F = \sqrt{2\pi n_e}$ and $E_F = \pi n_e/m^*$, our calculation further shows that the induced spin current is also insensitive to the electron density. Finally, it is addressed that with our material parameter, the numerical calculations indicate that the superconducting order parameter has little influence on the optical generations of both the spin polarization and spin current (not shown in Fig. 6).

[1] T. Yu and M. W. Wu, preceding paper, Phys. Rev. B **96**, 155311 (2017).
[2] J. L. Cheng and M. W. Wu, Appl. Phys. Lett. **86**, 032107 (2005).
[3] J. H. Jiang, M. W. Wu, and Y. Zhou, Phys. Rev. B **78**, 125309 (2008).
[4] M. W. Wu, J. H. Jiang, and M. Q. Weng, Phys. Rep. **493**, 61 (2010).
[5] L. E. Golub and E. L. Ivchenko, New J. Phys. **15**, 125003 (2013).
[6] T. Misawa, T. Yokoyama, and S. Murakami, Phys. Rev. B **84**, 165407 (2011).
[7] M. Sigrist and K. Ueda, Rev. Mod. Phys. **63**, 239 (1991).
[8] M. Eschrig, Phys. Today **64**(1), 43 (2011).
[9] J. Linder and T. Yokoyama, Phys. Rev. B **83**, 012501 (2011).
[10] I. Kulagina and J. Linder, Phys. Rev. B **90**, 054504 (2014).
[11] J. Linder and J. W. A. Robinson, Nat. Phys. **11**, 307 (2015).
[12] M. Eschrig, Rep. Prog. Phys. **78**, 104501 (2015).
[13] A. J. Leggett, *Quantum Liquids* (Oxford University Press, Oxford, 2006).
[14] A. J. Leggett, Rev. Mod. Phys. **47**, 331 (1975).
[15] A. D. Hillier, J. Quintanilla, B. Mazidian, J. F. Annett, and R. Cywinski, Phys. Rev. Lett. **109**, 097001 (2012).
[16] G. Tkachov, Phys. Rev. Lett. **118**, 016802 (2017).
[17] S. H. Jacobsen, I. Kulagina, and J. Linder, Sci. Rep. **6**, 23926 (2016).
[18] F. S. Bergeret, A. F. Volkov, and K. B. Efetov, Rev. Mod. Phys. **77**, 1321 (2005).
[19] A. I. Buzdin, Rev. Mod. Phys. **77**, 935 (2005).
[20] V. L. Berezinskii, ZhETF Pis. Red. **20**, 628 (1974) [JETP Lett. **20**, 287 (1974)].
[21] F. S. Bergeret and I. V. Tokatly, Phys. Rev. Lett. **110**, 117003 (2013); Phys. Rev. B **89**, 134517 (2014).
[22] A. D. Bernardo, S. Diesch, Y. Gu, J. Linder, G. Divitini, C. Ducati, E. Scheer, M. G. Blamire, and J. W. A. Robinson, Nat. Commun. **6**, 8053 (2015).
[23] Y. Kalcheim, O. Millo, A. D. Bernardo, A. Pal, and J. W. A. Robinson, Phys. Rev. B **92**, 060501(R) (2015).
[24] T. Yu and M. W. Wu, Phys. Rev. B **94**, 205305 (2016).
[25] H. Haug and A. P. Jauho, *Quantum Kinetics in Transport and Optics of Semiconductors* (Springer, Berlin, 1996).
[26] M. Levanda and V. Fleurov, J. Phys.: Condens. Matter **6**, 7889 (1994).
[27] T. Kita, Phys. Rev. B **64**, 054503 (2001).
[28] B. Y. Sun and M. W. Wu, New J. Phys. **15**, 083038 (2013).
[29] L. P. Gor'kov and G. M. Eliashberg, Zh. Eksp. Teor. Fiz. **51**, 612 (1968) [Sov. Phys.–JETP **27**, 328 (1968)].
[30] P. Lipavský, V. Špička, and B. Velický, Phys. Rev. B **34**, 6933 (1986).
[31] M. E. Peskin and D. V. Schroeder, *An Introduction to Quantum Field Theory* (Addison-Wesley, New York, 1995).
[32] Y. Nambu, Phys. Rev. **117**, 648 (1960).
[33] T. Yu and M. W. Wu, Phys. Rev. B **93**, 195308 (2016).
[34] L. P. Gor'kov and E. I. Rashba, Phys. Rev. Lett. **87**, 037004 (2001).
[35] E. Bauer, G. Hilscher, H. Michor, Ch. Paul, E. W. Scheidt, A. Gribanov, Yu. Seropegin, H. Noël, M. Sigrist, and P. Rogl, Phys. Rev. Lett. **92**, 027003 (2004).
[36] T. Yokoyama, Y. Tanaka, and J. Inoue, Phys. Rev. B **72**, 220504(R) (2005).
[37] Y. Tanaka, T. Yokoyama, A. V. Balatsky, and N. Nagaosa, Phys. Rev. B **79**, 060505(R) (2009).
[38] S. Takahashi and S. Maekawa, Phys. Rev. Lett. **88**, 116601 (2002).
[39] S. Takahashi and S. Maekawa, J. Phys. Soc. Jpn. **77**, 031009 (2008).
[40] H. Kontani, J. Goryo, and D. S. Hirashima, Phys. Rev. Lett. **102**, 086602 (2009).
[41] S. Takahashi and S. Maekawa, Jpn. J. Appl. Phys. **51**, 010110 (2012).
[42] T. Wakamura, H. Akaike, Y. Omori, Y. Niimi, S. Takahashi, A. Fujimaki, S. Maekawa, and Y. Otani, Nat. Mater. **14**, 675 (2015).
[43] H. L. Zhao and S. Hershfield, Phys. Rev. B **52**, 3632 (1995).
[44] S. Li, A. V. Andreev, and B. Z. Spivak, Phys. Rev. B **92**, 100506(R) (2015).

[45] A. G. Aronov, Yu. M. Galperin, V. L. Gurevich, and V. I. Kozub, in *Nonequilibrium Superconductivity*, edited by D. N. Langenberg and A. I. Larkin (Elsevier, New York, 1986).
[46] *Semiconductors*, Landolt-Börnstein, New Series, Vol. 17a, edited by O. Madelung (Springer, Berlin, 1987).
[47] J. M. Jancu, R. Scholz, E. A. de A. Silva, and G. C. La Rocca, Phys. Rev. B **72**, 193201 (2005).
[48] T. Yu and M. W. Wu, Phys. Rev. B **93**, 045414 (2016).
[49] H. Shiba, Prog. Theor. Phys. **40**, 435 (1968).
[50] J. Sinova, D. Culcer, Q. Niu, N. A. Sinitsyn, T. Jungwirth, and A. H. MacDonald, Phys. Rev. Lett. **92**, 126603 (2004).
[51] A. Khaetskii, Phys. Rev. B **73**, 115323 (2006).
[52] M. Glazov and A. Kavokin, J. Lumin. **125**, 118 (2007).
[53] K. Shen, R. Raimondi, and G. Vignale, Phys. Rev. B **90**, 245302 (2014).
[54] S. Wu and K. V. Samokhin, Phys. Rev. B **80**, 014516 (2009).
[55] H. Sumiyoshi and S. Fujimoto, J. Phys. Soc. Jpn. **82**, 023602 (2013).